

Directionality characteristics of horizontal response spectra from the 2022 M_W 6.9 Chihshang, Taiwan earthquake

Earthquake Spectra
XX(X):1–14
©The Author(s) 2024
Reprints and permission:
sagepub.co.uk/journalsPermissions.nav
DOI: 10.1177/87552930241247478
www.sagepub.com/



Alan Poulos,¹ M.EERI, and Eduardo Miranda,¹ M.EERI

Abstract

Horizontal earthquake ground motion intensity, and specifically response spectral ordinates, vary with orientation. This phenomenon is usually referred to as ground motion directionality and can be separated into two aspects: the orientation where the maximum spectral response occurs and the variation of response spectral ordinates as the orientation moves away from the orientation of maximum spectral response. This work studies both aspects using the recent 2022 M_W 6.9 Chihshang, Taiwan earthquake, which was recorded by a dense network of strong motion stations with various geological and topographical settings. The mean variation of response spectral ordinates with orientation is found to be slightly more significant than that of previous shallow crustal earthquakes in active tectonic regimes. Moreover, the orientation of maximum spectral response is found to be close to the transverse orientation, which is perpendicular to the orientation at a given site that points to the earthquake epicenter, confirming prior observations made for strike-slip earthquakes. These results suggest that the location of a site relative to the seismic source could be used to modify the outputs of ground motion models to estimate spectral responses at specific horizontal orientations.

Keywords

Directionality, Taiwan earthquake, ground motion intensity, response spectrum, strong motion

¹Department of Civil and Environmental Engineering, Stanford University, Stanford, CA, USA

Corresponding author:

Alan Poulos, Department of Civil and Environmental Engineering, Stanford University, 473 Via Ortega, Stanford, CA 94305, USA.
Email: apoulos@stanford.edu

Introduction

Horizontal earthquake ground motion intensity varies with orientation, a characteristic usually referred to as directionality. Several reasons have been given in the literature for the occurrence of ground motion directionality, such as local geologic heterogeneities (e.g., Bonamassa and Vidale 1991), topographic irregularities (e.g., Spudich et al. 1996), directivity effects (e.g., Somerville et al. 1997), basin edge effects (e.g., Heresi et al. 2020), and the finite duration of earthquake loading (e.g., Poulos et al. 2022).

For earthquake engineering purposes, ground motion intensity is usually characterized by response spectra. The directionality of this intensity measure can be separated into two aspects, the extent to which the intensity (i.e., the amplitude of a response spectral ordinate) varies with changes in orientation and the orientation at which the maximum intensity occurs. Previous studies have primarily focused on the extent of the variation of response spectral ordinates, which has typically been quantified only indirectly using ratios between different scalar definitions of the horizontal component (e.g., Beyer and Bommer 2006; Boore and Kishida 2017; Poulos and Miranda 2021), such as the ratio between the maximum and median intensities (usually known as RotD100 and RotD50, respectively, Boore 2010), or directly in a few studies by using the variation of spectral accelerations with changes in orientation with respect to the orientation of maximum intensity (e.g., Hong and Goda 2007; Shahi and Baker 2014; Poulos and Miranda 2022). The second aspect, that is, the orientation of maximum spectral response, has usually been studied only with respect to the earthquake strike due to concerns over directivity effects (e.g., Howard et al. 2005; Shahi and Baker 2014; Bradley and Baker 2015), which is an orientation common to all ground motions that recorded a given earthquake. These studies have found that, at locations very near to the earthquake source, the orientations of maximum spectral response are, on average, closer to the strike-normal than to the strike-parallel orientation. However, this strike-normal predominance of maximum intensity seems to disappear for rupture distances longer than approximately 5 km (Shahi and Baker 2014).

Recently, using records from shallow crustal earthquakes having magnitudes greater than or equal to five contained in the NGA-West2 database (Ancheta et al. 2014), Poulos and Miranda (2023) found that spectral accelerations of ground motions generated by strike-slip earthquakes have their maximum in orientations that are usually close to the transverse orientations, that is, an orientation perpendicular to the orientation at a given site that points to the earthquake epicenter. Unlike the strike-normal orientation, the transverse orientation changes from station to station depending on its location relative to the earthquake source.

Taiwan is located in a region of high seismicity where the Eurasia plate converges with the Philippine Sea plate. Consequently, earthquakes of significant magnitude strike the island regularly, especially close to its east coast (see Figure 1). On 18 September 2022 at 06:44 UTC, a M_w 6.9 earthquake occurred in the Longitudinal Valley in eastern Taiwan and was preceded by a M_w 6.5 earthquake that occurred approximately 17 hours before the mainshock. Unlike the well-known 1999 M_w 7.6 Chi-Chi earthquake, which had a reverse focal mechanism, the 2022 mainshock had a strike-slip focal mechanism (rake angle of 25° , USGS 2023) and occurred on two interacting crustal faults along the Longitudinal Valley suture, the west-dipping Central Ridge fault and the east-dipping Longitudinal Valley fault having a strike approximately parallel to the eastern coast of Taiwan (Lee et al. 2023; Tang et al. 2023). The dense network of strong motion digital accelerograph stations in Taiwan produced a rich set of records from this earthquake and therefore provides an excellent opportunity to study the directionality of earthquake ground motions, particularly the orientations of maximum spectral response.

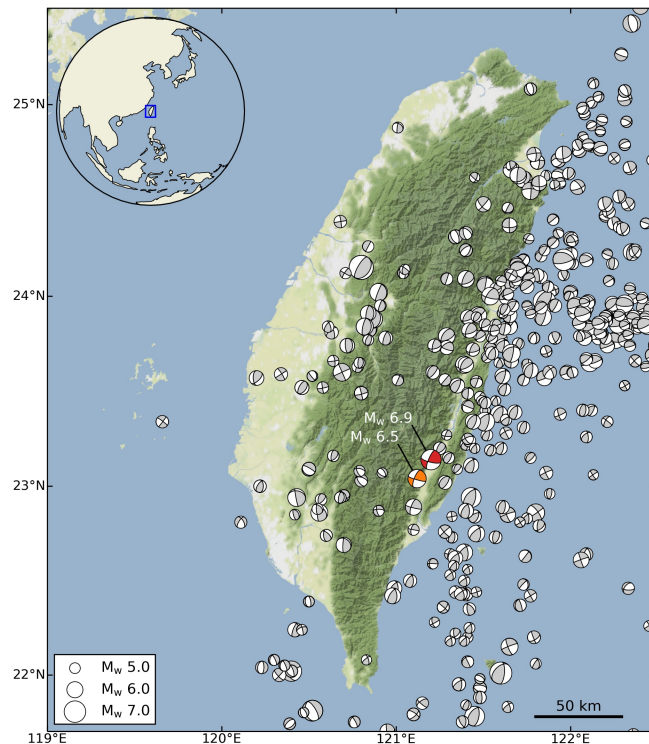


Figure 1. Focal mechanisms of $M_w \geq 5.0$ earthquakes from the Global Centroid Moment Tensor (CMT) catalog (Dziewonski et al. 1981; Ekström et al. 2012), for events since 1976. The sizes of the focal mechanisms indicate earthquake magnitude.

This work studies some directionality characteristics of ground motions recorded during the 2022 M_w 6.9 Chihshang, Taiwan earthquake. These characteristics are compared to recent observations from ground motions of the NGA-West2 strong ground motion database, specifically the orientation of maximum horizontal spectral response relative to the transverse orientation (Poulos and Miranda 2023) and the variation of normalized response spectral ordinates with changes in azimuth (Poulos and Miranda 2022), providing verification of these previous studies by taking advantage of this important new ground motion data set with diverse topographic settings and site conditions.

Data and Methods

The Taiwan Strong Motion Instrumentation Program (TSMIP) network has a large number of free-field strong-motion digital accelerograph stations throughout the island (Tsai and Lee 2005). Ground motion waveforms from TSMIP recorded during the 2022 earthquake were obtained from the Central Weather Bureau Seismographic Network (CWB Taiwan, 2010). Several of the strong-motion records had incomplete waveforms of the earthquake in one or both horizontal components. Thus, 30 records were

discarded. Moreover, three additional records were discarded because one of their horizontal components only recorded noise. The remaining 338 records were first instrument corrected and then bandpass filtered using a fourth-order Butterworth filter with corner frequencies of 0.05 and 35 Hz in both horizontal components.

For each record, the two orthogonal horizontal components were used to obtain bidirectional relative displacements of 161 linear elastic 5%-damped oscillators with linearly-spaced periods between 0 and 10 s. Figures 2b and 2c show the bidirectional relative displacements of 10-s oscillators subjected to two example ground motions from the 2022 M_w 6.9 Chihsiang, Taiwan earthquake, whose location is indicated in red and orange in the map shown in Figure 2a. The peak displacement (i.e., spectral displacement) of each oscillator in the horizontal plane (i.e., maximum from all non-redundant horizontal orientations) was then computed as follows:

$$Sd_{\text{RotD}100} = \max_t \sqrt{u_{\text{NS}}(t)^2 + u_{\text{EW}}(t)^2} \quad (1)$$

where $u_{\text{NS}}(t)$ and $u_{\text{EW}}(t)$ are the north-south and east-west histories of relative displacement, respectively, which are the orientations of horizontal recording sensors in all TSMIP network stations used herein. This peak displacement is a measure of ground motion intensity and was named RotD100 by Boore (2010). Equation (1) can be used with any pair of orthogonal horizontal orientations, not necessarily north-south and east-west, resulting in the same RotD100 intensity. However, using these orientations is convenient because the azimuth at which the RotD100 intensity occurs can be computed as:

$$\psi_{\text{RotD}100} = \arctan \left(\frac{u_{\text{NS}}(t_{\max})}{u_{\text{EW}}(t_{\max})} \right) \quad (2)$$

where t_{\max} is the time at which the peak displacement response from all orientations occurs, that is:

$$t_{\max} = \arg \max_t \sqrt{u_{\text{NS}}(t)^2 + u_{\text{EW}}(t)^2} \quad (3)$$

Note that the orientation where the RotD100 intensity occurs (Equation 2) is not the same as the principal components of ground motion based on the Arias intensity tensor (Arias 1970), and hence response spectral ordinates in these two orientations are also different (Hong and Goda 2010). Early studies on the orientation of principal components of ground motions found that one of these components is nearly vertical (e.g., Penzien and Watabe 1974; Kubo and Penzien 1979). Recent studies have found that the Arias intensity in the quasi-vertical principal component is typically only about 15%-20% of the trace of Arias intensity in shallow crustal earthquakes (Hong and Goda 2010). Therefore, in this study, the orientation of RotD100 is computed only within the horizontal plane without considering the vertical component, as horizontal components are the primary concern in earthquake-resistant design. While some studies have suggested that there is ample evidence of damage produced by the vertical component (e.g., Papazoglou and Elnashai 1996), the importance of the vertical component has continued to remain a subject of debate since direct evidence of damage from vertical motions is difficult to establish (e.g., Kunnath et al. 2008). Furthermore, even though most structures have not been explicitly designed to resist the vertical component, they have shown adequate performance during earthquakes, even when subjected to very large vertical accelerations. Although the study and inclusion of the vertical component might be important for some structures and in some situations, it is outside of the scope of this study.

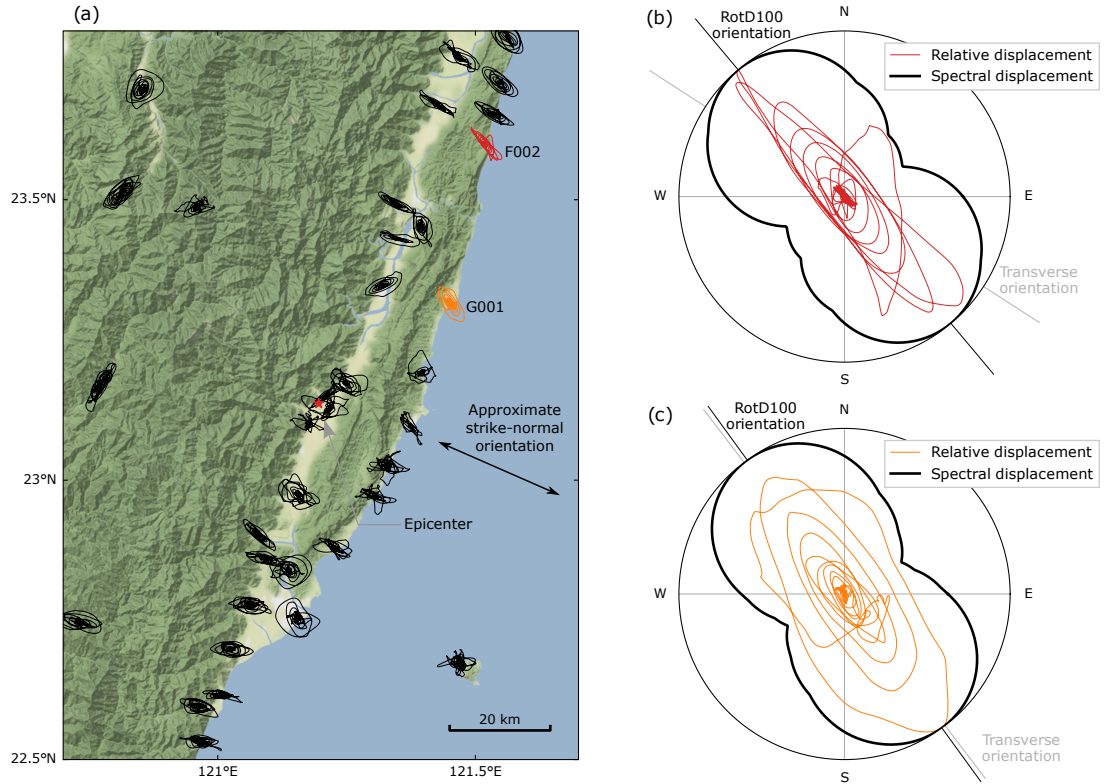


Figure 2. Normalized relative displacement hodograms of 5%-damped linear elastic oscillators with periods of 10 s subjected to the horizontal components of (a) ground motions recorded close to the epicenter and specific ground motions of recording stations (b) F002 and (c) G001 located at epicentral distances of 61 and 33 km, respectively.

Spectral displacements at any specific azimuth ψ can then be computed as the peak displacements of the oscillator within the specified azimuth as follows:

$$Sd(\psi) = \max_t |u_{NS}(t) \cos(\psi) + u_{EW}(t) \sin(\psi)| \quad (4)$$

Note that, because of the absolute value in Equation (4), $Sd(\psi)$ is a periodic function with a periodicity of 180° . Moreover, Equation (4) can also be used to compute RotD100 by taking the maximum from all azimuths:

$$Sd_{\text{RotD100}} = \max_{\psi \in [0, \pi]} \max_t |u_{NS}(t) \cos(\psi) + u_{EW}(t) \sin(\psi)| \quad (5)$$

and it is relatively easy to show that it is equivalent to using Equation (1), although significantly more computationally expensive because obtaining exactly the same intensity requires an algorithm to find locations of null derivatives of spectral ordinates with respect to changes in ψ .

In order to compare the variation of Sd with azimuth for ground motions of different intensities (i.e., $Sd_{\text{RotD}100}$) and different orientations of RotD100 (i.e., $\psi_{\text{RotD}100}$), a normalized spectral displacement is defined using the following ratio (Hong and Goda 2007):

$$\eta(\phi) = \frac{Sd(\psi_{\text{RotD}100} + \phi)}{Sd_{\text{RotD}100}} \quad (6)$$

where ϕ is an angle between the orientation of interest, ψ , and $\psi_{\text{RotD}100}$, that is, $\phi = \psi - \psi_{\text{RotD}100}$. Spectral displacements were also normalized by the median intensity from all non-redundant horizontal orientations as defined by Boore (2010), $Sd_{\text{RotD}50}$, because it is used by several recent ground motion models, resulting in the following ratio (Shahi and Baker 2014):

$$\nu(\phi) = \frac{Sd(\psi_{\text{RotD}100} + \phi)}{Sd_{\text{RotD}50}} \quad (7)$$

The $\eta(\phi)$ and $\nu(\phi)$ ratios were computed for all ground motion records and periods and are presented in the following section.

Results

The results are first shown for oscillators with periods of 5 and 10 s and then for all periods between 0 and 10 s. Figure 2a shows the relative displacement responses of 10-s oscillators subjected to both horizontal ground motion components from records relatively close to the epicenter. In order to focus on the directionality of responses and not the relative intensity at different stations, the bidirectional displacements are normalized by $Sd_{\text{RotD}100}$, such that all hodograms have equal maximum displacement from the resting position of the oscillator. As shown in the figure, most responses are significantly polarized, that is, their amplitudes tend to be much larger in certain orientations. Moreover, their maximum amplitudes tend to occur at consistent orientations, and these orientations tend to be close to the transverse orientation, as can be seen in more detail in the example hodograms presented in Figures 2b and 2c for two sites whose locations are indicated in color in Figure 2a. For stations along the Longitudinal Valley, where the transverse orientation is very close to strike-normal orientation, the orientation of maximum response also tends to occur near the strike-normal orientation. However, for stations with other source-to-site azimuths, the orientations of maximum response depart from the strike-normal orientation and remain relatively close to the transverse orientation.

Because of the normalization used in the hodograms of Figure 2a, ground motion intensities between sites cannot be compared using the figure. Thus, Figure 3 shows $Sd_{\text{RotD}100}$ for a period of 10 s of the records before normalization/scaling. The intensities at this period of 10 s are higher on the east coast of Taiwan near the epicenter and also significantly high on some parts of the island's west coast. Ground motions recorded in the north and south of the island have significantly lower intensities.

The orientations of maximum intensity, that is, of peak relative displacement computed using Equation (2), are shown in Figure 4 for oscillators with periods of 5 and 10 s. These orientations, represented in Figure 4 by black lines at each site, are compared to the transverse orientation, represented by gray lines. To simplify the visual comparison of these orientations, the angular distance between these two orientations, $|\alpha|$, is indicated by the color of the circle at each site. The empirical probability distribution of $|\alpha|$ for each period is also presented in the upper left corner of each corresponding panel of Figure

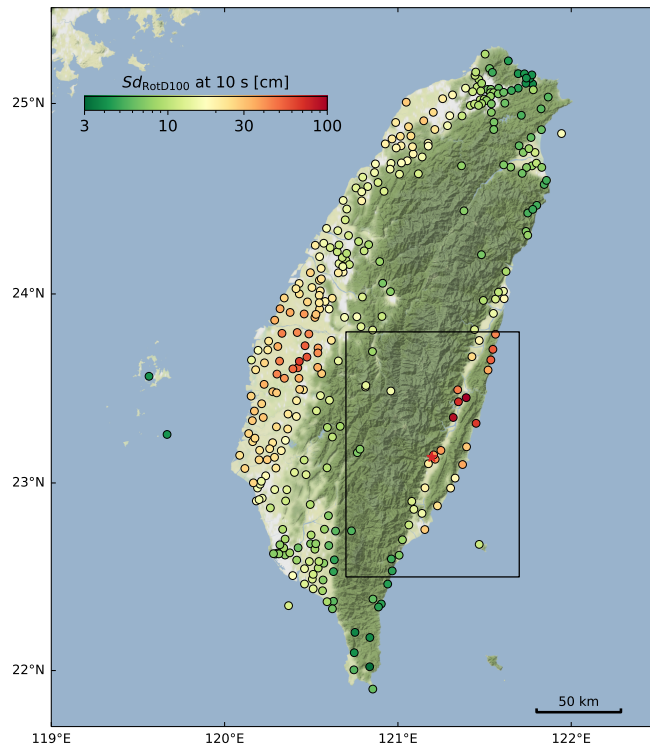


Figure 3. Peak relative displacements within the horizontal plane ($Sd_{RotD100}$) of oscillators with periods of 10 s subjected to recorded ground motions. The black rectangle represents the extent of Figure 2a.

4 using angular increments of 5° . If all orientations of maximum intensity were equally likely, as currently assumed in design standards in the U.S. for distances longer than 5 km (ASCE 2022), the distributions would be close to a uniform probability distribution. However, Figure 4 shows that the empirical distributions have a distinct higher density at lower angles, with mean values significantly lower than the 45° mean of a uniform probability distribution. This means that, in this earthquake, the orientation of maximum intensity tends to be close to the transverse orientation, consistent with prior observations by Poulos and Miranda (2023) for strike-slip earthquakes with $M_W \geq 5.0$ in the NGA-West2 ground motion database. Moreover, the orientations of maximum intensity are closer to the transverse orientation for the 10 s case than for 5 s, with the mean angular distance between the two orientations for the two periods being 18.7° and 31.4° , respectively.

Similar probability distributions to those shown in Figure 4 are presented in Figure 5, but now for angle α , that is, now distinguishing between angles that are clockwise and counterclockwise rotations away from the transverse orientation. As shown, both distributions (i.e., for 5 and 10 s) are relatively symmetric with respect to $\alpha = 0^\circ$ (i.e., the transverse orientation) and have their highest density close to this orientation. The figure also compares the distributions to those fitted by Poulos and Miranda (2023)

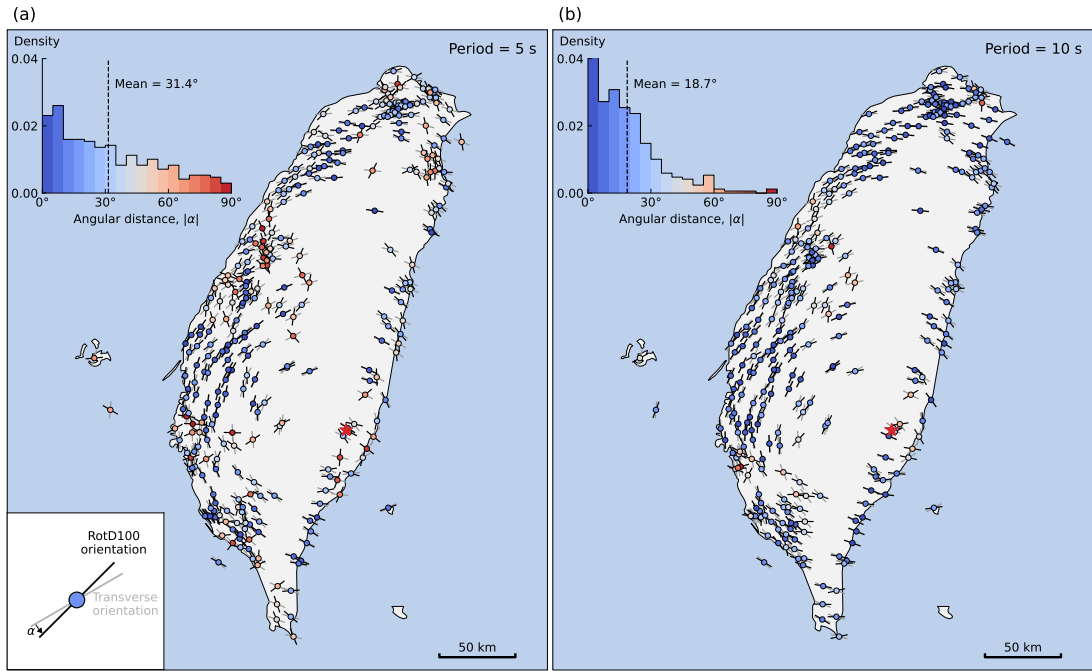


Figure 4. Orientations of RotD100 for 5%-damped oscillators with periods of (a) 5 s and (b) 10 s. Circles represent the locations of recording stations, short black lines represent orientations of RotD100, and short gray lines represent transverse orientations. The angular difference between the transverse orientation and the orientation of RotD100 is given by α . The absolute value of α is indicated by the color of the circles, and its empirical probability distribution for both periods is given by the corresponding histogram in the upper left of each panel.

using ground motions of the NGA-West2 database from strike-slip earthquakes with $M_w \geq 5.0$, showing that the distributions are fairly similar. However, the α angles from the Taiwan earthquake are somewhat closer to the transverse orientation for these periods.

To evaluate the possible effect of site conditions, Figure 6 shows the angular distances $|\alpha|$ for oscillators having periods of 5 and 10 s as a function of the average shear-wave velocity of the upper 30 m of soil (V_{s30}) at each station. The $|\alpha|$ values were averaged in bins according to their associated V_{s30} values, showing that the mean $|\alpha|$ has no statistically significant trend with V_{s30} . This suggests that site effects do not play a significant role in the observed phenomenon of the orientations of RotD100 being close to the transverse orientation.

The values of $|\alpha|$ were also computed for all periods between 0 and 10 s, resulting in the period-dependent statistics shown in Figure 7. The mean, median, and percentiles shown in the figure tend to decrease as the period becomes longer, which means that the orientation of maximum spectral response gets closer to the transverse orientation as the period increases. At very short periods, the empirical distribution of $|\alpha|$ is close to a uniform distribution, with the mean value being close to that of a uniform

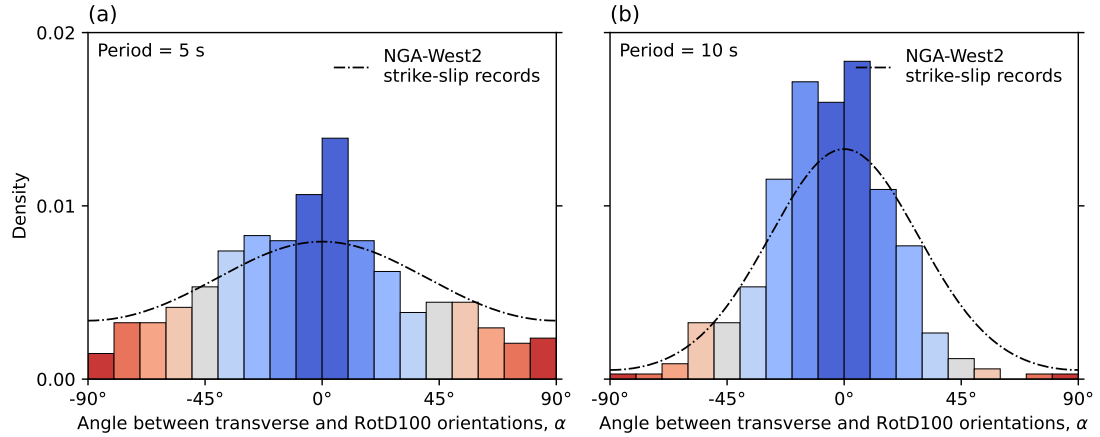


Figure 5. Distribution of angles between the transverse orientation and the orientation of RotD100 for (a) 5 s and (b) 10 s. The probability distributions of NGA-West2 records from strike-slip earthquakes were obtained from Poulos and Miranda (2023).

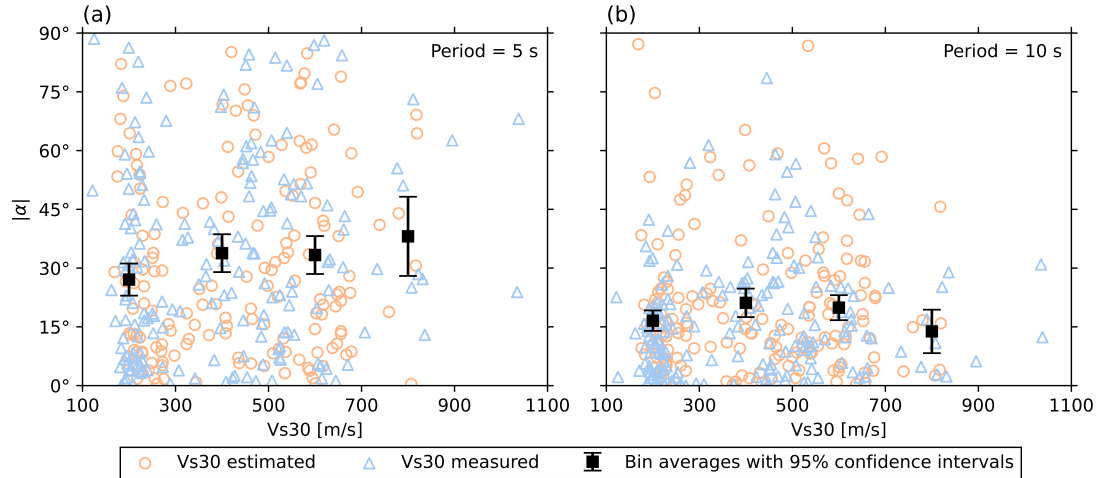


Figure 6. Angular distance between the transverse orientation and the orientation of RotD100 for (a) 5 s and (b) 10 s, as a function of the Vs30 values of the station. The averages are taken for bins of Vs30 with widths of 200 m/s and the error bars correspond to 95% confidence intervals.

distribution (i.e., 45°), whereas at long periods most of the records have $|\alpha|$ values much lower than 45° . For example, for periods greater than 8 s, approximately 90% of the records have $|\alpha| < 45^\circ$, and approximately half of the records have $|\alpha| < 15^\circ$. Figure 7 also shows the mean obtained previously for ground motions of strike-slip earthquakes from the NGA-West2 database (Poulos and Miranda 2023).

At short periods the mean is relatively similar; however, for periods greater than approximately 5 s, the mean from the 2022 Chihshang, Taiwan earthquake is lower than that of the Poulos and Miranda (2023), with the difference ranging from approximately 4° to 9° .

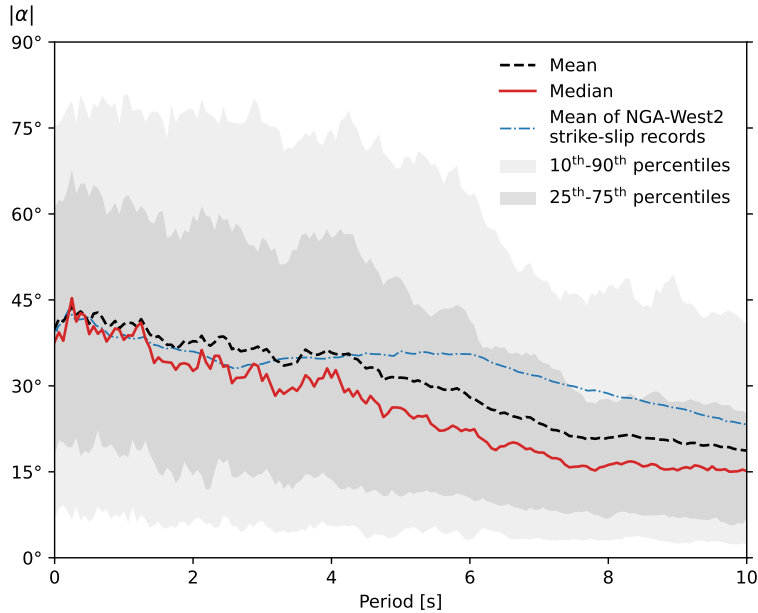


Figure 7. Statistics of the angular distance between the orientation of RotD100 and the transverse orientation, $|\alpha|$, as a function of the oscillator period. Mean values of NGA-West2 records were obtained from Poulos and Miranda (2023) and were computed using $M_w \geq 5.0$ earthquakes with strike-slip faulting.

Figure 8 presents spectral displacements for the same two periods computed for all ground motions normalized by the RotD100 and RotD50 intensity using Equations (6) and (7), respectively. The figure also presents the mean normalized spectral displacements as a function of angle ϕ and compares them to those obtained from records of the NGA-West2 database (Poulos and Miranda 2022). The mean values are very similar for both periods, with the differences usually only being perceptible for orientations close to the orientation perpendicular to the orientation of RotD100. For the orientation that is perpendicular to the orientation of RotD100 (i.e., $\phi = -90^\circ$ or $\phi = 90^\circ$), the mean η values from the 2022 Chihshang, Taiwan ground motion records are 7.2% and 6.4% lower than those of the NGA-West2 database for periods of 5 and 10 s, respectively, indicating that records from this earthquake are slightly more polarized than the mean level of polarization of records in the NGA-West2 database.

Conclusions

This paper studied two directionality characteristics of horizontal spectral displacements using ground motions recorded during the 2022 M_w 6.9 Chihshang earthquake in eastern Taiwan. One of these

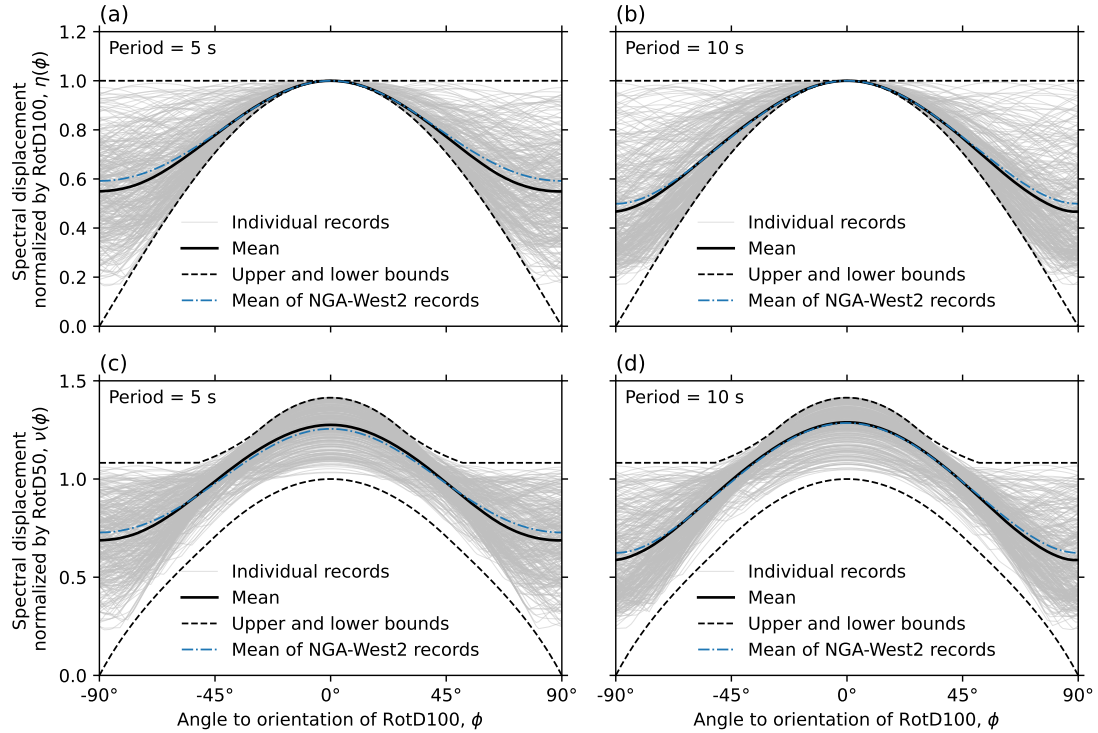


Figure 8. Variation of spectral displacement normalized by (a and b) RotD100 and (c and d) RotD50 as a function of the angle to the orientation of RotD100 for (a and c) 5 s and (b and d) 10 s. The mean $\eta(\phi)$ and $\nu(\phi)$ values of NGA-West2 records were obtained from Poulos and Miranda (2022).

characteristics is the average variations of spectral displacement with changes in orientation, which is slightly more significant than that obtained by averaging records within the NGA-West2 database from several previous shallow crustal earthquakes (Poulos and Miranda 2022). These differences could be attributed to the style of faulting of this earthquake (i.e., strike-slip), which tends to produce ground motion records with spectral displacements at long periods that, on average, vary more with changes in orientation than those generated by earthquakes with other styles of faulting. Future studies could identify if these variations also depend on typical predictor variables considered by ground motion model, such as magnitude or distance, which could explain some of the small differences observed between this earthquake and the mean NGA-West2 values.

The second investigated directionality characteristic is the orientation of maximum spectral response, which is found to occur close to the transverse orientation, consistent with previous observations (Poulos and Miranda 2023; Girmay et al. 2024a,b). This is observed to be the case for ground motions recorded at stations with various topographic settings, such as in mountains and basins and in various site conditions. Moreover, the mean angular distance between the transverse orientation and the orientation of maximum

spectral response decreases as the period gets longer. For example, the mean is 31.4° at 5 s and 18.7° at 10 s. These values are significantly lower than the 45° mean angular distance that would occur if maximum spectral responses were equally likely to occur in any horizontal orientation (i.e., with a uniform probability distribution). These results confirm that the location of a site relative to the seismic source of a strike-slip earthquake primarily controls the orientation where horizontal spectral responses are expected to be stronger or weaker than those predicted by ground motion models, and therefore this relative location can be considered to improve the estimates of spectral responses at specific horizontal orientations in future seismic hazard analyses. This is especially important for earthquake-resistant design, where most structures have two principal horizontal orientations and their seismic response is primarily controlled by the ground motion intensity at these orientations.

Data and Resources

TSMIP strong-motion records were obtained from the Taiwan Seismic and Geophysical Data Management System at <https://gdmsn.cwb.gov.tw> (last accessed October 2022). The Vs30 values of the recording stations were obtained from the Engineering Geological Database for TSMIP at <https://egdt.ncree.org.tw> (last accessed October 2022), where most of the measured Vs30 values are from Kuo et al. (2012). Some map figures used tiles by Stamen Design, under CC BY 3.0, and basemap data by OpenStreetMap, under ODbL.

Acknowledgements

Financial support to the first author to conduct doctoral studies at Stanford University has been provided by the National Agency for Research and Development (ANID) / Doctorado Becas Chile under grant 2019-72200307 and the Nancy Grant Chamberlain Fellowship from the Department of Civil and Environmental Engineering at Stanford University. The authors thank the Taiwan Strong Motion Instrumentation Program (TSMIP) and the Central Weather Bureau Seismographic Network for gathering, processing, and distributing the ground motion records used in this study.

Declaration of conflicting interests

The authors declared no potential conflicts of interest with respect to the research, authorship, and/or publication of this article.

References

- Ancheta TD, Darragh RB, Stewart JP, Seyhan E, Silva WJ, Chiou BSJ, Wooddell KE, Graves RW, Kottke AR, Boore DM et al. (2014) NGA-West2 database. *Earthquake Spectra* 30(3): 989–1005.
- Arias A (1970) A measure of earthquake intensity. In: Hansen RJ (ed.) *Seismic Design for Nuclear Power Plants*. Cambridge, MA: MIT Press, pp. 438–483.
- ASCE (2022) *Minimum design loads and associated criteria for buildings and other structures*. ASCE/SEI 7-22 edition. Reston, VA: American Society of Civil Engineers.
- Beyer K and Bommer JJ (2006) Relationships between median values and between aleatory variabilities for different definitions of the horizontal component of motion. *Bulletin of the Seismological Society of America* 96(4A): 1512–1522.

- Bonamassa O and Vidale JE (1991) Directional site resonances observed from aftershocks of the 18 October 1989 Loma Prieta earthquake. *Bulletin of the Seismological Society of America* 81(5): 1945–1957.
- Boore DM (2010) Orientation-independent, nongeometric-mean measures of seismic intensity from two horizontal components of motion. *Bulletin of the Seismological Society of America* 100(4): 1830–1835.
- Boore DM and Kishida T (2017) Relations between some horizontal-component ground-motion intensity measures used in practice. *Bulletin of the Seismological Society of America* 107(1): 334–343.
- Bradley BA and Baker JW (2015) Ground motion directionality in the 2010–2011 Canterbury earthquakes. *Earthquake Engineering & Structural Dynamics* 44(3): 371–384.
- Central Weather Bureau (CWB, Taiwan) (2012) Central Weather Bureau Seismographic Network. DOI:10.7914/SN/T5. URL <https://www.fdsn.org/networks/detail/T5/>.
- Dziewonski AM, Chou TA and Woodhouse JH (1981) Determination of earthquake source parameters from waveform data for studies of global and regional seismicity. *Journal of Geophysical Research: Solid Earth* 86(B4): 2825–2852.
- Ekström G, Nettles M and Dziewoński A (2012) The global CMT project 2004–2010: Centroid-moment tensors for 13,017 earthquakes. *Physics of the Earth and Planetary Interiors* 200: 1–9.
- Girmay N, Miranda E and Poulos A (2024a) Orientation and intensity of maximum response spectral ordinates during the December 20, 2022 Mw 6.4 Ferndale, California earthquake. *Soil Dynamics and Earthquake Engineering* 176: 108323.
- Girmay N, Poulos A and Miranda E (2024b) Directionality and polarization of response spectral ordinates in the 2023 Kahramanmaraş, Türkiye earthquake doublet. *Earthquake Spectra* 40(1): 486–504.
- Heresi P, Ruiz-García J, Payán-Serrano O and Miranda E (2020) Observations of Rayleigh waves in Mexico City Valley during the 19 September 2017 Puebla–Morelos, Mexico earthquake. *Earthquake Spectra* 36(2S): 62–82. DOI:10.1177/8755293020942547.
- Hong HP and Goda K (2007) Orientation-dependent ground-motion measure for seismic-hazard assessment. *Bulletin of the Seismological Society of America* 97(5): 1525–1538.
- Hong HP and Goda K (2010) Characteristics of horizontal ground motion measures along principal directions. *Earthquake Engineering and Engineering Vibration* 9(1): 9–22.
- Howard JK, Tracy CA and Burns RG (2005) Comparing observed and predicted directivity in near-source ground motion. *Earthquake Spectra* 21(4): 1063–1092.
- Kubo T and Penzien J (1979) Analysis of three-dimensional strong ground motions along principal axes, San Fernando earthquake. *Earthquake Engineering & Structural Dynamics* 7(3): 265–278.
- Kunnath SK, Erduran E, Chai YH and Yashinsky M (2008) Effect of near-fault vertical ground motions on seismic response of highway overcrossings. *Journal of Bridge Engineering* 13(3): 282–290.
- Kuo CH, Wen KL, Hsieh HH, Lin CM, Chang TM and Kuo KW (2012) Site classification and Vs30 estimation of free-field TSMIP stations using the logging data of EGDT. *Engineering Geology* 129: 68–75.
- Lee SJ, Liu TY and Lin TC (2023) The role of the west-dipping collision boundary fault in the Taiwan 2022 Chihshang earthquake sequence. *Scientific Reports* 13: 3552.
- Papazoglou AJ and Elnashai AS (1996) Analytical and field evidence of the damaging effect of vertical earthquake ground motion. *Earthquake Engineering & Structural Dynamics* 25(10): 1109–1137.
- Penzien J and Watabe M (1974) Characteristics of 3-dimensional earthquake ground motions. *Earthquake Engineering & Structural Dynamics* 3(4): 365–373.

- Poulos A and Miranda E (2021) Relations between MaxRotD50 and some horizontal components of ground-motion intensity used in practice. *Bulletin of the Seismological Society of America* 111(4): 2167–2176.
- Poulos A and Miranda E (2022) Probabilistic characterization of the directionality of horizontal earthquake response spectra. *Earthquake Engineering & Structural Dynamics* 51(9): 2077–2090.
- Poulos A and Miranda E (2023) Effect of style of faulting on the orientation of maximum horizontal earthquake response spectra. *Bulletin of the Seismological Society of America* DOI:10.1785/0120230001.
- Poulos A, Miranda E and Baker JW (2022) Evaluation of earthquake response spectra directionality using stochastic simulations. *Bulletin of the Seismological Society of America* 112(1): 307–315.
- Shahi SK and Baker JW (2014) NGA-West2 models for ground motion directionality. *Earthquake Spectra* 30(3): 1285–1300.
- Somerville PG, Smith NF, Graves RW and Abrahamson NA (1997) Modification of empirical strong ground motion attenuation relations to include the amplitude and duration effects of rupture directivity. *Seismological Research Letters* 68(1): 199–222.
- Spudich P, Hellweg M and Lee WHK (1996) Directional topographic site response at Tarzana observed in aftershocks of the 1994 Northridge, California, earthquake: implications for mainshock motions. *Bulletin of the Seismological Society of America* 86(1B): S193–S208.
- Tang CH, Lin YN, Tung H, Wang Y, Lee SJ, Hsu YJ, Shyu JBH, Kuo YT and Chen HY (2023) Nearby fault interaction within the double-vergence suture in eastern Taiwan during the 2022 Chihshang earthquake sequence. *Communications Earth & Environment* 4: 333.
- Tsai YB and Lee CP (2005) Strong motion instrumentation programs in Taiwan: past and present. In: Gürkan P and Anderson JG (eds.) *Directions in strong motion instrumentation*. Dordrecht, The Netherlands: Springer, pp. 255–278.
- USGS (2023) M 6.9 - 90 km E of Yujing, Taiwan. Available at: <http://earthquake.usgs.gov/earthquakes/eventpage/us7000i90q>. Accessed November 2023.